CrossMark

electronic reprint

Acta Cryst B

STRUCTURAL SCIENCE
CRYSTAL ENGINEERING
MATERIALS

ISSN: 2052-5206
journals.iucr.org/b

$CH_3NH_3PbI_3$: precise structural consequences of water absorption at ambient conditions

Alla Arakcheeva, Dmitry Chernyshov, Massimo Spina, László Forró and Endre Horváth

Acta Cryst. (2016). B**72**, 716–722

Acta Cryst B
STRUCTURAL SCIENCE
CRYSTAL ENGINEERING
MATERIALS

ISSN 2052-5206

$CH_3NH_3PbI_3$: precise structural consequences of water absorption at ambient conditions

Alla Arakcheeva,[a]* Dmitry Chernyshov,[b] Massimo Spina,[a] László Forró[a] and Endre Horváth[a]

[a]Laboratory of Physics of Complex Matter, Ecole polytechnique Fédérale de Lausanne, CH-1015 Lausanne, Switzerland, and [b]SNBL, ESRF, 71 Avenue des Martyrs, 38043 Grenoble CEDEX 9, France. *Correspondence e-mail: alla.arakcheeva@epfl.ch

Received 19 April 2016
Accepted 27 June 2016

Edited by M. Dusek, Academy of Sciences of the Czech Republic, Czech Republic

Keywords: hybrid organic–inorganic lead iodide; hydrogen bonding; aged $MAPbI_3$; perovskite; solar cells.

CCDC references: 1487955; 1487956

Supporting information: this article has supporting information at journals.iucr.org/b

The crystal structure of the pristine (I) and aged (II) crystals of $CH_3NH_3PbI_3$ (hereafter $MAPbI_3$) hybrid organic–inorganic lead iodide has been studied at 293 K with high-precision single-crystal X-ray diffraction using a synchrotron light source. We show that (I) and (II) are characterized by an identical tetragonal unit cell but different space groups: $I422$ for (I) and $P4_22_12$ for (II). Both space groups are subgroups of $I4/mcm$, which is widely used for $MAPbI_3$. The main difference between (I) and (II) comes from the difference in hydrogen bonds between the MA^+ cation and the PbI_3 framework which is the direct consequence of H_2O insertion in the aged crystal (II).

1. Introduction

Organic–inorganic hybrid perovskite $CH_3NH_3PbI_3$ ($MAPbI_3$) is currently under precise investigation owing to its application in solar cells (Kojima *et al.*, 2009; Im *et al.*, 2011; Service, 2013; Snaith, 2013; Grätzel, 2014; Spina *et al.*, 2015; Bi *et al.*, 2016; Chang *et al.*, 2016; Hodes & Cahen, 2014). The crystal structure of this compound contains a methyl ammonium (MA^+) cation, $[H_3C{-}NH_3]^+$, in the cuboctahedral interstices of the framework formed by $[PbI_6]$ octahedra. Only weak N—H···I hydrogen bonds fix this linear cation in the coordination of 12 I atoms. Hence, statistical disorder over different orientations and short-range correlations for some of them can be expected for the MA^+ linear cation in such a coordination. These specific features result in a high flexibility of the structure's symmetry depending on conditions, both external (pressure, temperature) and internal (hydrogen bonds stabilizing by the electronic state of I atoms; Lee *et al.*, 2015; Weller *et al.*, 2015). Indeed, two temperature-dependent phase transitions were reported for $MAPbI_3$: cubic → tetragonal at 330 K and tetragonal → orthorhombic at 161 K (Stoumpos *et al.*, 2013; Baikie *et al.*, 2013). The different tetragonal space groups, such as $I4/mcm$ (Kawamura *et al.*, 2002; Yamada *et al.*, 2015; Dang *et al.*, 2015; Weller *et al.*, 2015), $I4cm$ (Stoumpos *et al.*, 2013; Xie *et al.*, 2015) and $I4/m$ (Baikie *et al.*, 2013), were reported even in the room-temperature phase. The hydrogen bonds have never been studied experimentally using the X-ray diffraction (XRD) technique. Weller *et al.* (2015) localized H atoms in the tetragonal phase based on powder neutron diffraction experiments at room temperature. However, the non-realistic C—N—H = 84, 84 and 70° angles and a too short N—H = 0.67 Å distance called for more detailed investigations.

It is a well known fact that $MAPbI_3$ is structurally unstable at room temperature. Gradual decomposition can always be observed in air and its rate essentially scales with increasing

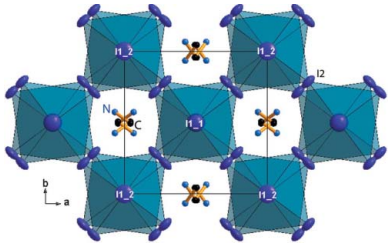

Table 1
Experimental details.

	(I) (pristine crystal)	(II) (aged crystal)
Crystal data		
Chemical formula	PbI_3 (CH_6N)	$PbI_{3-x}(CH_6N)_{1-x}(H_2O)_y$ [x = 0.05 (3); y = 0.09 (2)]
M_r	619.97	616.41
Crystal system, space group	Tetragonal, $I422$	Tetragonal, $P4_22_12$
Temperature (K)	293	293
a, c (Å)	8.88375 (18), 12.7010 (3)	8.8829 (3), 12.7008 (4)
V (Å^3)	1002.38 (5)	1002.17 (7)
Z	4	4
Radiation type	Synchrotron, λ = 0.68362 Å	Synchrotron, λ = 0.68362 Å
μ (mm^{-1})	23.28	23.23
Crystal size (mm)	0.0025 × 0.0020 × 0.0015	0.0025 × 0.0020 × 0.0015
Data collection		
Diffractometer	Dectris-*CrysAlis PRO*-abstract goniometer imported dectris images diffractometer	Dectris-*CrysAlis PRO*-abstract goniometer imported dectris images diffractometer
Absorption correction	Multi-scan	Multi-scan
T_{min}, T_{max}	0.582, 1.000	0.399, 1.000
No. of measured, independent and observed [$I > 3\sigma(I)$] reflections	4261, 773, 721	17 735, 4191, 1704
R_{int}	0.029	0.071
$(\sin\theta/\lambda)_{max}$ (Å^{-1})	0.759	0.766
Refinement		
$R[F > 3\sigma(F)]$, $wR[F > 3\sigma(F)]$, S	0.012, 0.015, 1.19	0.041, 0.058, 1.52
No. of reflections	773	4191
No. of parameters	67	195
No. of restraints	1	2
H-atom treatment	H-atom parameters softly constrained	H-atom parameters softly constrained
$\Delta\rho_{max}$, $\Delta\rho_{min}$ (e Å^{-3})	0.40, −0.36	0.66, −0.88
Absolute structure	305 of Friedel pairs used in the refinement	1031 of Friedel pairs used in the refinement
Absolute structure parameter	0.25 (13)	0.09 (5)

Computer programs: *CrysAlisPro* (Agilent, 2014), *SUPERFLIP* (Palatinus & Chapuis, 2007), *JANA*2006 (Petříček *et al.*, 2014), *DIAMOND* (Brandenburg & Putz, 2005).

air humidity. A mechanism for the $MAPbI_3$ crystal structure transformation and its decomposition induced by its exposure to air is very important for understanding the compound's stabilization, its applications and crystal engineering. Xie *et al.* (2015) excluded oxidation as a reason for the decomposition. They show that the crystal structures of the pristine sample and the aged one in dry air are identical. Shirayama *et al.* (2016) investigated a phase transformation occurring near the surface of ultra-smooth $MAPbI_3$ layers in humid air. They show evidence that the $MAPbI_3$ degradation can be associated with the formation of PbI_2 and a $MAPbI_3$ hydrate. However, any structural study of the $MAPbI_3$ crystal aged in wet air has been missing up to now.

This article fills this gap. The synchrotron radiation XRD experiments performed with an aged crystal exposed to humidity and other high-quality freshly prepared pristine crystals uncover the symmetry changes, the hydrogen-bond patterns and the main differences between the two crystals.

2. Experimental

2.1. Synthesis and crystallization

The pristine $CH_3NH_3PbI_3$ single crystals (from 5 to 8 mm down to submicron size) were prepared by precipitation from a concentrated aqueous solution of hydriodic acid (57 w% in H_2O, 99.99% Sigma–Aldrich) containing lead(II) acetate trihydrate (99.999%, Acros Organics) and a corresponding amount of CH_3NH_2 solution (40 w% in H_2O, Sigma–Aldrich). A constant 328–315 K temperature gradient was applied to induce saturation of the solute in the low-temperature region of the solution. After 24 h, submillimeter-sized flake-like nuclei were floating on the surface of the solution. Large cube-like and rhombohedral $MAPbI_3$ crystals with 3–5 mm silver-grey facets were obtained after 7 d. The aged crystals were obtained after keeping the pristine ones in air of 98% H_2O humidity over 2 h at room temperature.

2.2. X-ray diffraction studies

Collections of experimental data of single-crystal diffraction intensities were obtained at room temperature with the radiation wavelength λ = 0.68362 Å using the PILATUS@SNBL diffractometer at the Swiss–Norwegian Beam Lines, European Synchrotron Radiation Facility (Dyadkin *et al.*, 2016). *CrysAlisPro* (Agilent, 2014) and *JANA*2006 (Petříček *et al.*, 2014) were used for the experimental data processing and structural calculations, respectively. Other experimental details are listed in Table 1 and are available from the CIF in the supporting information.

2.2.1. Details of reciprocal space affecting the results of the structure refinements. Both the pristine (I) and aged (II)

Table 2
Hydrogen-bond characteristics in the pristine (I) and aged (II) crystals.

	(I) $PbI_3(CH_6N)$	(II) $PbI_{3-x}(CH_6N)_{1-x}(H_2O)_y$ [x = 0.05 (3); y = 0.09 (2)]	
Presence of the cation $MA^+ = [CH_3NH_3]^+$ (%)	100	33	59
N—H···*A*	N—H1*n*···I2	N1—H1*n*1···I1_2	N2—H1*n*2···I1_2
H···*A* (Å)	3.18	2.88	2.84
N—*A* (Å)	4.017 (17)	3.76 (5)	3.79 (4)
A—H···*D* angle (°)	141.93	146.48	158.44
N—H···*A*	N—H2*n*···I2	N1—H2*n*1···I1_1	N2—H2*n*2···I1_1
H···*A* (Å)	3.00	3.09	3.03
N—*A* (Å)	3.99 (2)	3.93 (5)	4.02 (4)
A—H···*D* (°)	173.69	142.64	167.76
N—H···*A*	N—H3*n*···I2	N1—H3*n*1···I2	N2—H3*n*2···I2
H···*A* (Å)	3.18	3.06	3.22
N—*A* (Å)	3.92 (2)	3.95	3.94
A—H···*D* (°)	131.83	149.20	130.18
N—H···*A*	N—H3*n*···I1_1		
H···*A* (Å)	3.07		
N—*A* (Å)	3.85		
A—H···*D* angle (°)	135.68		

crystals show similar tetragonal unit-cell parameters (Table 1). Reciprocal space reconstructions of (I) demonstrate the perfect quality of the crystal studied (Fig. 1, left). The images of (II) (Fig. 1, right) contain reflections of six twin components. Three of them are linked by the threefold axis of the perovskite-type unit cell, which is quite common for related compounds of lower symmetry. The centre of symmetry links the three others. According to our final structure refinement, the twin components have the following mass–matrix description: 27% – (1 0 0/0 1 0/0 0 1); 13% – ($\frac{1}{2}\ \frac{1}{2}\ 1/\frac{1}{2}\ \frac{1}{2}\ -1/-\frac{1}{2}\ \frac{1}{2}\ 0$); 16% – ($\frac{1}{2}\ -\frac{1}{2}\ 1/-\frac{1}{2}\ \frac{1}{2}\ 1/-\frac{1}{2}\ -\frac{1}{2}\ 0$); 9% – ($-1\ 0\ 0/0\ -1\ 0/0\ 0\ -1$); 12% – ($-\frac{1}{2}\ -\frac{1}{2}\ -1/-\frac{1}{2}\ -\frac{1}{2}\ 1/\frac{1}{2}\ -\frac{1}{2}\ 0$); 23% – ($-\frac{1}{2}\ \frac{1}{2}\ -1/\frac{1}{2}\ -\frac{1}{2}\ -1/\frac{1}{2}\ \frac{1}{2}\ 0$). Unlike (I), crystal (II) displays the image which clearly shows additional powder diffraction rings (Fig. 1, right). Those rings suggest that some additional nucleation centres have been formed, mostly on the surface of crystal (II). The nucleation is associated with the partial decomposition of $MAPbI_3$ accompanied by the formation of a polycrystalline PbI_2 phase, traces of which have been detected in our powder diffraction experiments performed for the aged crystals. Diffuse scattering lines (Fig. 1, right) indicate some structural disorder, which can be associated with the insertion of the H_2O molecules in the crystal structure of (II). The presence of the powder rings, the diffuse scattering and twinning explain the somewhat lower quality of the refinement for (II) (R = 0.0411) in comparison to (I) (R = 0.112).

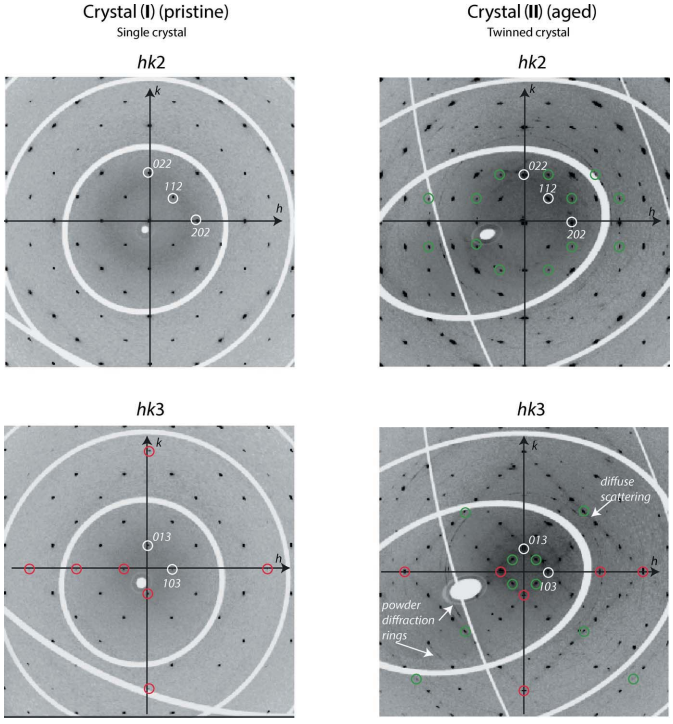

Figure 1
*hk*2 and *hk*3 reciprocal space sections of the pristine and aged crystals. Red circles surround some of the *h*03 and 0*k*3 reflections violating the condition h, k, $l = 2n$ for 0*kl* and *h*0*l* reflections. These reflections are incompatible with the alternating *c* and *b* glide planes in the tetragonal space groups *I*4/*mcm* of both the pristine and aged crystals. Green circles surround some reflections violating the condition $h + k + l = 2n$. These reflections are incompatible with the *I* centring of the unit cell in the aged crystal. Diffuse scattering lines and powder diffraction rings are well visible in the aged crystal images.

2.2.2. Space-group determination, structure refinement and chemical composition of the pristine crystal. The collection of experimental data contains no reflections violating the *I*-centring of the unit cell. The Laue class *I*4/*mmm* is confirmed by R_{int} = 0.029. In the data collection, 66/267 observed/all reflections violate the *I*4/*mcm* and *I*4*cm* space groups commonly considered for (I). These reflections are incompatible with the *c*-glide planes; the red circles in Fig. 1, left panel, indicate some of them. Hence, only two space groups, *I*422 and $I\bar{4}2m$, can be considered as subgroups of *I*4/*mcm* in the *I*4/*mmm* Laue class. The best results have been obtained in *I*422. The absence of any forbidden reflections, low R indices [$R(F)$ = 0.0112, $wR(F)$ = 0.0115] and small variability of residual electron density values ($\Delta\rho_{max}$ = 0.40, $\Delta\rho_{min}$ = −0.36 e Å^{-3}, which are observed in the 2 Å vicinity of the I

and Pb positions) confirm the *I*422 space group of (I) (Table 1).

The atomic parameters of Pb and I are identical in both tested space groups. However, the selected *I*422 space group allows the localization of a split position of the $MA^+ = [H_3C—NH_3]^+$ cation. C and N have been localized from a series of residual electron-density calculations. Figs. 2 and 3(*a*) illustrate the localization. The distances C—N = 1.40 (3) Å were softly constrained in the final refinement. The H atoms were found near N and C from the residual electron density calculated after refinement of Pb, I, C and N. The distances C—H = 1.0 (1) Å and N—H = 1. 0 (1) Å were softly constrained in the final refinement together with the tetrahedron angles: N—C—H1*c* = H1*c*—C—H2*c* = H1*c*—C—H3*c* = H2*c*—C—H3*c* = C—N—H1*n* = H1*n*—N—H2*n* = H1*n*—N—H3*n* = H2*n*—N—H3*n* = 109.47°. Four different orientations of one $MA^+ = [H_3C—NH_3]^+$ cation are statistically distributed around the site 4*d*: $(0\,\frac{1}{2}\,\frac{1}{2})$ with a probability of 25% for each orientation fitting the sum occupancy $o(MA^+) = 4 \times 25 = 100\%$. These orientations are shown in Figs. 4(*a*) and (*b*). As expected, the main hydrogen bonds between the cation and I atoms correspond to the $NH_3\cdots I$ connections. The characteristics of these bonds are listed in Table 2.

The nominal chemical composition has been confirmed by refinements of the atomic position occupancies, which show the values *o*(I1_1) = *o*(I1_2) = 1.02 (2), *o*(I2) = 1.01 (1) and $o(MA^+)$ = 1.02 (4) with fixed *o*(Pb) = 1. These values have been fixed as 1.0 during the final refinement. The atomic displacements of Pb and I have been refined in the anharmonic approximation using a tensor of the 5th rank. All refined atomic parameters of (I) are deposited in CIF format in the supporting information.

2.2.3. Space-group determination, structure refinement and chemical composition of the aged crystal. The experimental data collection contains 368/4550 (about 20%) observed/all reflections violating the *I* centring of the unit cell. This estimation takes into account the effect of the twinning described above. Similar to the pristine crystal (I), an essential set of reflections is incompatible with the *c*-glide plane of symmetry. Some of them are marked in Fig. 1, right panel. No reflections contradict the 4_2 and the coordinate 2_1 symmetry axes. Hence, the space group $P4_22_12$ has been considered for the structure refinement of (II) (Table 1). The low enough *R*

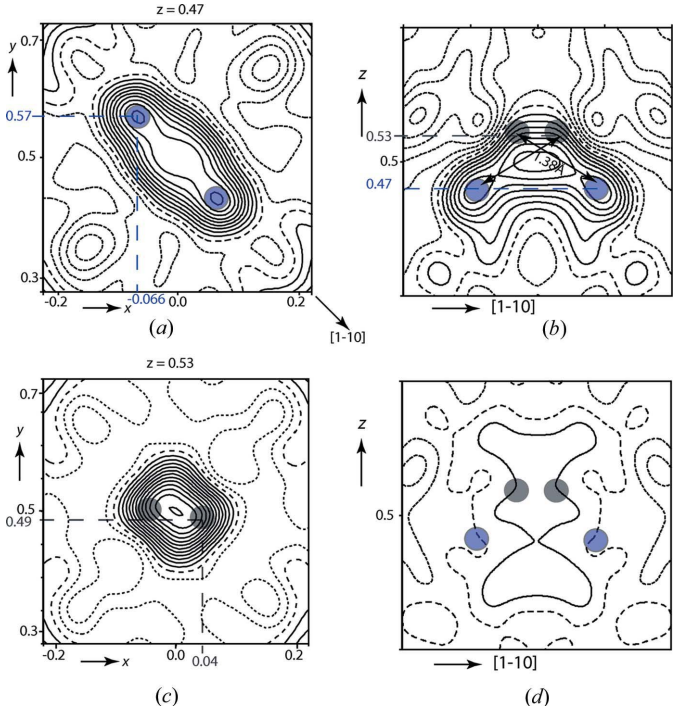

Figure 2
Illustration of the N (blue) and C (grey) atoms' localization with the residual electron density mapping in the pristine crystal structure. The shown sections are calculated in the 4 Å vicinity of the (0 0.5 0.5) point of the unit cell. The solid dashed and striped lines correspond to positive, negative and zero contours, respectively, drawn with a step of 0.05 e $Å^{-3}$. (*a*) and (*b*) The maps were calculated after the refinement of Pb and I atoms. The starting atomic coordinates of one symmetrically independent N atom are indicated in blue. The two shown N positions are connected by the twofold axis parallel to *c*. (*c*) The indicated starting coordinates of C have been checked after refinement of N, Pb and I atoms. (*d*) The map obtained after refinement of Pb, I, N and C atoms contains no maxima, which justifies the correct localization of N and C.

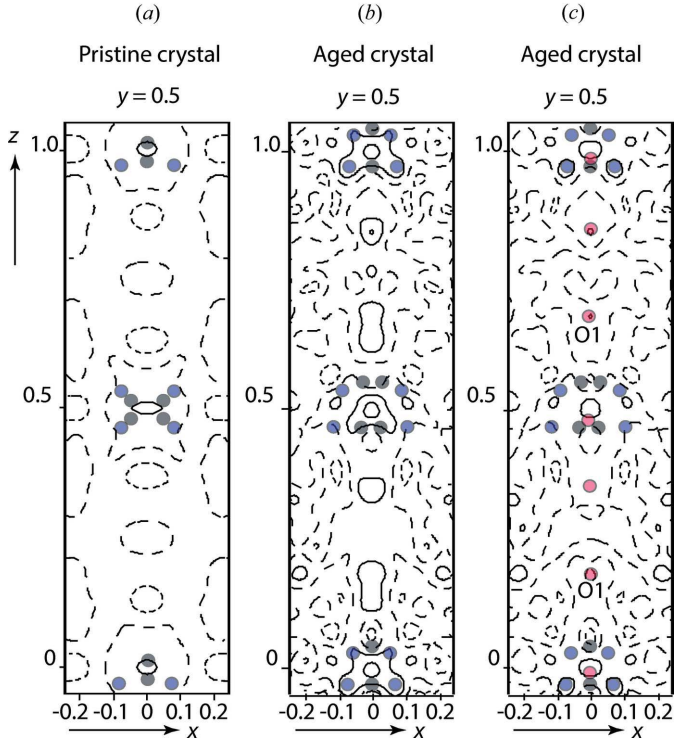

Figure 3
Illustration of the O (H_2O) localization in the aged crystal using the electron density mapping. The shown section is calculated in the vicinity of the 4_2 axis $(0\,\frac{1}{2}\,z)$ for (*a*) the pristine and (*b*), (*c*) aged crystals. The sections (*a*) and (*b*) calculated after refinements of Pb, I, C, N and H differ by extra maxima in the 4_2 axis of the aged crystal. The section (*c*) was calculated after fitting those maxima by partially occupied O (red circles). O1 indicates the most probable position of 0.088 (18) refined occupancy. The solid dashed and striped lines correspond to positive, negative and zero contours, respectively, drawn with a step of 0.2 e $Å^{-3}$. The projections of C (grey) and N (blue) atoms are shown as well.

indices [$R(F) = 0.0411$, $wR(F) = 0.058$] and small variability of the residual electron density values ($\Delta\rho_{max} = 0.66$, $\Delta\rho_{min} = -0.88$ e Å^{-3}, which is observed in the 2 Å vicinity of I and Pb atoms), justify this space group.

The atomic coordinates of Pb and I in the aged crystal (II) are very similar to those in the pristine one. However, their atomic displacement parameters are essentially higher in (II). These displacements were therefore refined with the anharmonic tensor of the 6th rank. The localization of C, N and H atoms of two symmetrically non-equivalent MA^+ cations was performed similarly to that in (I). Similar to (I), the distances C—N = 1.40 (6), C—H = 1.0 (1) and N—H = 1.0 (1) Å were softly constrained in the final refinement. In contrast to the pristine crystal (I), the residual electron density calculated after the localization shows some extra maxima for (II) (Figs. 3*a* and *b*), which can be associated with a disordered distribution of H_2O. These maxima are observed in the (0 0.5 *z*) 4_2 axis (Fig. 3*b*), which runs through the centres of the MA^+ cations. The occupancy of the most probable position of O (Fig. 3*c*) has been refined to 0.088 (18). The occupancy of other O positions is within one standard deviation.

The chemical composition of (II) has been estimated by refinements of the atomic position occupancies. Fixing o(Pb) = 1.0, occupancies of three I and two MA^+ symmetrically non-equivalent positions were refined. One I position showed o(I1_1) = 0.96 (2) < 1, while others appear as fully occupied. The refined occupancies of two MA^+ non-equivalent cations differ as 0.167 (12) and 0.295 (12). It means that four orientations of the cation are distributed non-randomly around each centre of its location. The sum occupancy $o(MA^+) = 2 \times 0.167\ (12) + 2 \times 0.295\ (12) = 0.92\ (5) < 1$. These orientations are shown in Figs. 4(*c*) and (*d*). Finally, the chemical composition of (II) can be written as $PbI_{3-x}(CH_6N)_{1-x}(H_2O)_y$, where $x = 0.05$ (3) and $y = 0.09$ (2).

Similar to the pristine crystal (I), the main hydrogen bonds between the cations and I atoms correspond to the $(NH_3)\cdots$I connections. The characteristics of these bonds are listed in Table 2 separately for two non-equivalent cation positions. All refined atomic parameters of (II) are deposited in CIF format and shown in Table S2 of the supporting information.

3. Results and discussion

Despite the newly defined space groups, the unit-cell parameters of both (I) and (II) are very similar to the published ones by Kawamura *et al.* (2002), Yamada *et al.* (2015), Dang *et al.* (2015), Weller *et al.* (2015), Stoumpos *et al.* (2013), Xie *et al.* (2015) and Baikie *et al.* (2013) for the room-temperature tetragonal phase. Atomic positions of Pb and I found in our study in the unit cell are also practically identical to all of these publications. Similar to Weller *et al.* (2015), we found that the MA^+ cation is statistically disordered over four of its different orientations. Unlike Weller *et al.* (2015), which processed the structure refinement in the *I*4/*mcm* space group, we found reasonable positions not only for C and N, but also for H atoms connected to them in the pristine crystal (I) at room temperature using the proven space group *I*422. It could be mentioned that for the powder, even the neutron diffraction data cannot distinguish between centrosymmetric and non-centrosymmetric space groups. For the first time, the crystal structure of the aged crystal (II) has also been solved. That allows us to shed light on the $MAPbI_3$ decomposition in wet air conditions.

Comparative analysis of (I) and (II) shows their topological similarity and differences (Fig. 4), which can be understood as a direct consequence of H_2O insertion in the aged crystal (II). As can be deduced from Fig. 5, inserting the H_2O moves the I2 atoms slightly apart and transforms the system of hydrogen bonds between MA^+ cations and a set of I atoms. Some of the N—H$\cdots$I hydrogen bonds ($\sim$ 9%) in the pristine crystal (I) switch to a very short interaction distance H—O(H_2O) = 1.16 Å in

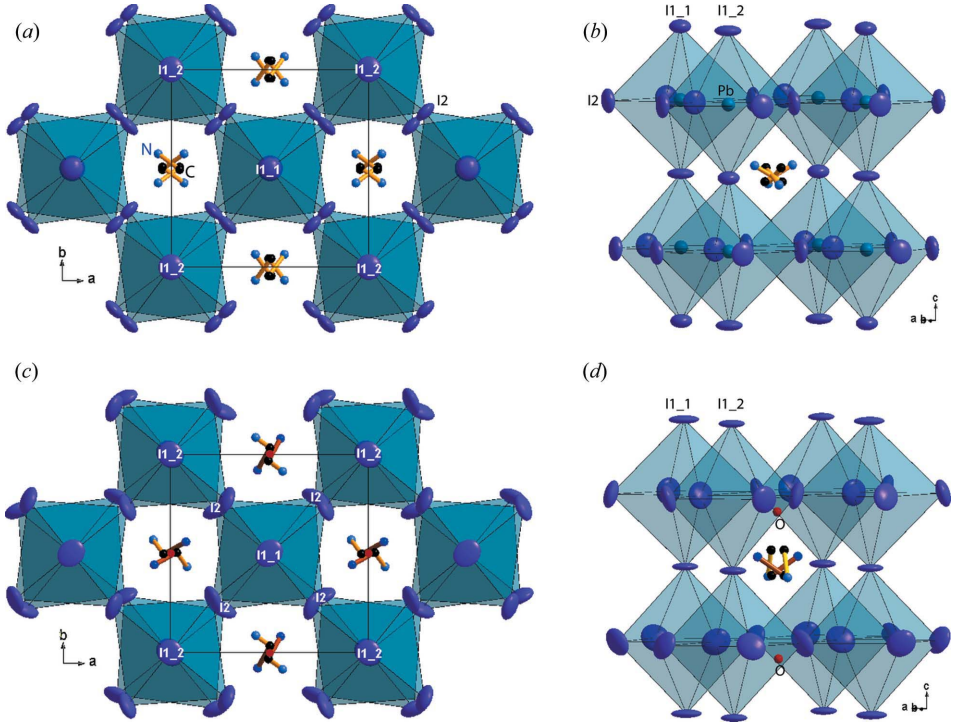

Figure 4
Comparison of the pristine (I) and the aged (II) specific features of their crystal structures. The ellipsoids (100% probability) of I atoms and orientations of MA^+ cations (lines connecting C and N) are shown. In (I), (*a*) and (*b*), four different orientations (yellow lines) are statistically present with a probability of 25% at each centre of I12-cuboctahedron. In (II), (*c*) and (*d*), two of four orientations are present with 29.5% probability (red lines) and two others are present with 16.5% probability (yellow lines). The most probable position of O (H_2O) is shown in red for (II).

the aged crystal (II). This can be considered as a reason for the pristine crystal decomposition in the following way. Comparing the H_2O and MA^+ position occupancies (Table S2 in the supporting information), one can say that their sum is equal to 1 within one standard deviation. This can be interpreted as the fact that H_2O replaces an MA^+ cation. Such a replacement destroys the structure owing to an imbalance in charge. Indeed, replacement of an MA^+ cation by a neutral H_2O molecule requires the removal of the corresponding amount of I^- anions. This leads to nucleation of PbI_2 and this phase can be identified in the powder diffraction rings in the reciprocal space reconstructions (Fig. 1). In other words, the replacement of an MA^+ cation by a neutral H_2O molecule initiates and supports a process for the compound distortion. This decomposition can be described by the following chemical reaction: $CH_3NH_3PbI_3 + (H_2O) = CH_3NH_2\uparrow + PbI_2\downarrow + (H^+ + I^- + H_2O)$. The asymmetrically inserted H_2O interacts with the MA^+ cation. This creates different preferences for its four orientations (Fig. 5*b*). The difference in the four orientations leads to the change of the space group from *I*422 (I) to $P4_22_12$ (II). The partial structure distortions and decomposition consequently affect atomic displacements of all the atoms especially of (I), which can be observed an increase of their atomic displacement ellipsoids (Figs. 4 and 5). The observation of rods of diffuse scattering indicates a disorder of planar objects; such a disorder indicates that H_2O inserts are not random but correlated (Fig. 1*b*).

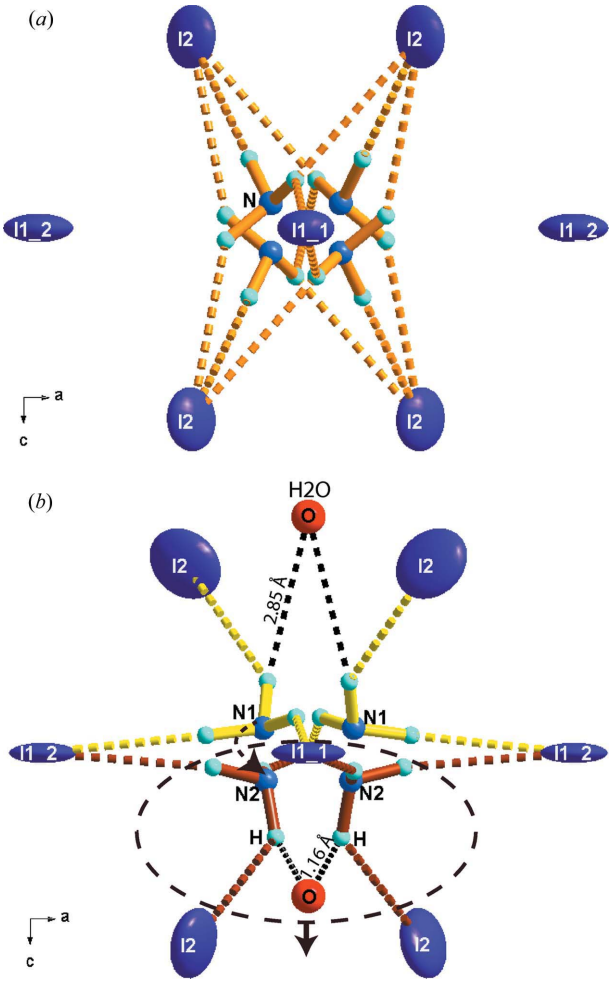

Figure 5
Comparison of the hydrogen bonds in (*a*) the pristine (I) and (*b*) the aged (II) crystals. The system of the N—H···I hydrogen bonds connecting the $[CH_3NH_3]^+$ cation with the (Pb,I)-framework is shown. The four shown N atoms correspond to the four orientations of the cation. Three corresponding H atoms are shown for each N position. In (I) (*a*), all 12 hydrogen bonds (orange lines) are statistically present with a probability of 25% for each one. In (II) (*b*), six bonds (brown lines) corresponding to cation 2 (N2) are present with 29.5% probability and six bonds (yellow lines) corresponding to cation 1 (N1) are present with 16.5% probability for each. The O—H interactions (black dotted lines) are present with a probability of 8.8%. The probabilities of the bonds are defined by the probability of the cation orientations and the O occupancy. The dashed black contour indicates the most probable part of the structure, which leads to its decomposition. The dashed black arrow between N1 and N2 indicates the compensation of the leaving part.

Summarizing the contribution of the present study, we found that the difference between the pristine and the crystal aged in wet air appears as a direct consequence of H_2O insertion in the aged crystal. The H_2O inserts change the system of hydrogen bonds between MA^+ cation and I atoms. This is accompanied by the change of the *I*422 space group, characteristic of the pristine crystal, into $P4_22_12$, characteristic of the aged crystal. We also found that a partial occupancy of the H_2O positions induces vacancies observed for the MA^+ cation and I atoms in the aged crystal. We also note short-range correlations in the disordered $P4_22_12$ form as manifested in the structured diffuse scattering. These results provide the solid experimental ground necessary for the understanding of the degradation processes in this new family of solar cell materials.

Acknowledgements

This study was supported by the project H2020-ERC, grant number 10306/670918 and the ERC Advanced Grant Picoprop.

References

Agilent (2014). *CrysAlisPro*, Version 1.171.37.35. Agilent Technologies, Yarnton, England.
Baikie, T., Fang, Y., Kadro, J. M., Schreyer, M., Wei, F., Mhaisalkar, S. G., Graetzel, M. & White, T. J. (2013). *J. Mater. Chem. A*, **1**, 5628–5641.
Bi, D., Tress, W., Dar, M. I., Gao, P., Luo, J., Renevier, C., Schenk, K., Abate, A., Giordano, F., Chang, S. H., Lin, K.-F., Cheng, H.-M., Chen, C.-C., Wu, W.-T., Chen, W.-N., Wu, P.-J., Chen, S.-H. & Wu, C.-G. (2016). *Sci. Adv.* **2**, e1501170, 1–7.
Brandenburg, K. & Putz, H. (2005). *DIAMOND*, Version 3. Crystal Impact GbR, Bonn, Germany.
Chang, S. H., Lin, K.-F., Cheng, H.-M., Chen, C.-C., Wu, W.-T., Chen, W.-N., Wu, P.-J., Chen, S.-H. & Wu, C.-G. (2016). *Solar Energy Mater. Solar Cells*, **145**, 375–381.
Dang, Y., Liu, Y., Sun, Y., Yuan, D., Liu, X., Lu, W., Liu, G., Xia, H. & Tao, X. (2015). *CrystEngComm*, **17**, 665–670.
Dyadkin, V., Pattison, P., Dmitriev, V. & Chernyshov, D. (2016). *J. Synchrotron Rad.* **23**, 825–829.
Grätzel, M. (2014). *Nat. Mater.* **13**, 838–842.
Hodes, G. & Cahen, D. (2014). *Nature Photon*, **8**, 87–88.
Im, J.-H., Lee, C.-R., Lee, J.-W., Park, S.-W. & Park, N.-G. (2011). *Nanoscale*, **3**, 4088–4093.

Kawamura, Y., Mashiyama, H. & Hasebe, K. (2002). *J. Phys. Soc. Jpn*, **71**, 1694–1697.
Kojima, A., Teshima, K., Shirai, Y. & Miyasaka, T. (2009). *J. Am. Chem. Soc.* **131**, 6050–6051.
Lee, J.-H., Bristowe, N. C., Bristowe, P. D. & Cheetham, A. K. (2015). *Chem. Commun.* **51**, 6434–6437.
Palatinus, L. & Chapuis, G. (2007). *J. Appl. Cryst.* **40**, 786–790.
Petříček, V., Dusek, M. & Palatinus, L. (2014). *Z. Kristallogr.* **229**, 345–352.
Service, R. F. (2013). *Science*, **342**, 794–797.
Shirayama, M., Kato, M., Miyadera, T., Sugita, T., Fujiseki, T., Hara, S., Kadowaki, H., Murata, D., Chikamatsu, M. & Fujiwara, H. (2016). *J. Appl. Phys.* **119**, 115501.
Snaith, H. J. (2013). *J. Phys. Chem. Lett.* **4**, 3623–3630.
Spina, M., Lehmann, M., NáFrádi, B., Bernard, L., Bonvin, E., Gaál, R., Magrez, A., Forró, L. & Horváth, E. (2015). *Small*, **11**, 4824–4828.
Stoumpos, C. C., Malliakas, C. D. & Kanatzidis, M. G. (2013). *Inorg. Chem.* **52**, 9019–9038.
Weller, M. T., Weber, O. J., Henry, P. F., Di Pumpo, A. M. & Hansen, T. C. (2015). *Chem. Commun.* **51**, 4180–4183.
Xie, J., Liu, Y., Liu, J., Lei, L., Gao, Q., Li, J. & Yang, S. (2015). *J. Power Sources*, **285**, 349–353.
Yamada, Y., Yamada, T., Phuong, L. Q., Maruyama, N., Nishimura, H., Wakamiya, A., Murata, Y. & Kanemitsu, Y. (2015). *J. Am. Chem. Soc.* **137**, 10456–10459.